EFFECTIVE SIMULATION OF A MACROSCOPIC MODEL FOR STATIONARY MICROMAGNETICS

CARSTEN CARSTENSEN AND DIRK PRAETORIUS

ABSTRACT. The effective behaviour of stationary micromagnetic phenomena is modelled by a convexified Landau-Lifshitz minimization problem for the limit of large and soft magnets Ω without the exchange energy. The numerical simulation of the resulting minimization problem has to overcome difficulties caused by the pointwise side-restriction $|\mathbf{m}| \leq 1$ and the stray field energy on the unbounded domain $\mathbb{R}^d$. A penalty method models the side-restriction and the exterior Maxwell equation is recast via a nonlocal integral operator $\mathcal{P}$. As shown in [7, 21], the discretization leads to a nonlocal problem with piecewise constant ansatz and test functions and (dense) stiffness matrices with closed form formulae for their entries. This paper addresses the numerical solution with Newton-Raphson schemes and the scientific computation of effective micromagnetic simulations.

1. INTRODUCTION

Stationary micromagnetic phenomena of static or quasi-static processes are usually based on a variational model named after Landau and Lifshitz [3, 13]. The magnetic body Ω is a bounded Lipschitz domain in $\mathbb{R}^d$ for $d = 2, 3$ on which the microscopic vector-valued magnetization

$$\mathbf{m}_\alpha : \Omega \to \mathbb{R}^d$$

minimizes the magnetic energy $E_\alpha(\mathbf{m})$ subject to the side-restriction $|\mathbf{m}| = $ constant that depends on the temperature. The effective magnetization vector $\mathbf{m} : \Omega \to \mathbb{R}^d$ is a spatial average of the microscopic magnetization $\mathbf{m}_\alpha$ and so averages out the small oscillations which $\mathbf{m}_\alpha$ is enforced to develop for small values of the exchange energy parameter $\alpha \geq 0$. For large and soft magnets, the parameter α vanishes in the magnetic energy

$$(1.1) \qquad E_\alpha(\mathbf{m}) := \int_\Omega \phi(\mathbf{m})\,dx - \int_\Omega \mathbf{f} \cdot \mathbf{m}\,dx + \frac{1}{2}\int_{\mathbb{R}^d} |\nabla u|^2\,dx + \alpha \int_\Omega |\nabla \mathbf{m}|^2\,dx.$$

This is justified in [9] where it is proven that the effective model for $\alpha \to 0$ is $E_0(\mathbf{m})$ where the effective magnetization $\mathbf{m} : \Omega \to \mathbb{R}^d$ obeys the averaged side-restriction $|\mathbf{m}| \leq 1$ (with the aforementioned constant normalized to 1). Notice that the approximation even of an effective magnetization zero is a nontrivial highly oscillatory problem [14, 16, 17, 20, 24, 26]. In contrast to that, this paper follows [8, 7, 21] and adopt the effective model directly. This relaxed problem (RP) [9, 26] reads: Minimize

$$(1.2) \qquad E_0^{**}(\mathbf{m}) := \int_\Omega \phi^{**}(\mathbf{m})\,dx - \int_\Omega \mathbf{f} \cdot \mathbf{m}\,dx + \frac{1}{2}\int_{\mathbb{R}^d} |\nabla u|^2\,dx$$

subject to the side-restriction

$$(1.3) \qquad\qquad |\mathbf{m}(x)| \leq 1 \quad \text{for almost every } x \in \Omega.$$

Given some direction $\mathbf{e} \in \mathbb{R}^d$, called easy axis, $|\mathbf{e}| = 1$, and an orthonormal basis $(\mathbf{e}, \mathbf{z}_2, \mathbf{z}_3, \ldots, \mathbf{z}_d)$ of $\mathbb{R}^d$, i.e. $\mathbf{z}_2, \ldots, \mathbf{z}_d$ are an orthonormal basis of the orthogonal complement of span$\{\mathbf{e}\}$, the (uniaxial) anisotropic energy density ϕ^{**}, e.g. of Cobalt, in (1.2) reads

$$(1.4) \qquad\qquad \phi^{**}(\mathbf{m}) = \frac{1}{2} \sum_{j=2}^{d} (\mathbf{m} \cdot \mathbf{z}_j)^2 \quad \text{for all } \mathbf{m} \in \mathbb{R}^d.$$

This specifies the first term out of three of (1.2) and we restrict to the uniaxial case in the following. The second is a linear relation with the applied magnetization $\mathbf{f}$, a given function in $L^2(\Omega; \mathbb{R}^d)$; here and below we employ standard notation for Lebesgue spaces, e.g. $\mathbf{f} \in L^2(\Omega)$ means that $\mathbf{f}$ is measurable (i.e. the pointwise limit of some sequence of continuous functions) and L^2 integrable (i.e. $\int_\Omega |\mathbf{f}(x)|^2 \, dx < \infty$) while $L^2(\Omega; \mathbb{R}^d)$ means $L^2(\Omega) \times \cdots \times L^2(\Omega)$ in d components. The third term in (1.2) models the stray field energy in $\mathbb{R}^d$. Given a magnetization $\mathbf{m}$ (as the argument in $E_0^{**}(\mathbf{m})$) the associated magnetic potential u allows a Laplace operator Δu to equal zero outside Ω, equals div $\mathbf{m}$ in a weak sense in Ω, and involves a Neumann boundary condition $\partial u/\partial \mathbf{n} = \mathbf{m} \cdot \mathbf{n}$ along $\partial \Omega$ (in a weak form), where $\mathbf{n}$ denotes the outer normal on the boundary $\partial \Omega$. Thus, u is a function of $\mathbf{m}$ defined by

$$(1.5) \qquad\qquad \Delta u = \text{div } \mathbf{m} \quad \text{in } \mathbb{R}^d \text{ in the sense of distributions.}$$

Here and below, $\mathbf{m}$ is an L^∞ function on Ω and extended by zero outside the magnetic domain Ω. Then, ∇u is uniquely determined and belongs to $L^2(\mathbb{R}^d; \mathbb{R}^d)$ and hence the third energy term is finite. This concludes the short description of the effective model via (RP). In fact, (RP) has solutions [9] which are unique [7, 20, 21]. The numerical simulation of the effective magnetization as a minimizer in (RP) already overcame the severe difficulty of highly oscillating micromagnetizations. But there remain the convex side-restriction $|\mathbf{m}| \leq 1$ and the unbounded domain $\mathbb{R}^d$ in the far field equation.

A coupling of the piecewise constant discretization of the effective magnetizations $\mathbf{m}_h$ with a (nonconforming) finite element discretization of the magnetic potentials u_h in [8] required a bounded domain $\widehat{\Omega}$ that surrounds the magnetic body Ω. Therein, a penalty scheme successfully treated the side-restriction $|\mathbf{m}_h| \leq 1$. In [7, 16, 17, 21], the exterior problem is equivalently recast utilizing integral operators. This paper reviews the full model and its discretization with an a priori and a posteriori error analysis in Section 2. The focus is then on the performance of the simple Newton-Raphson scheme with penalty term in a multilevel framework of adaptive mesh-refining algorithms. Section 3 defines the numerical algorithms proposed while Section 4 and Section 5 reports on numerical tests and general conclusions about the performance. A numerical example from [7] with known exact solution and a scientific computing experiment from [8] with a practical application are treated. A short Section 6 summarizes a few observations and comments on future developments.

2. Exact and discrete models and a priori and a posteriori error control

This section presents the exact effective model proposed for the numerical simulation of the macroscopic magnetization vector $\mathbf{m} \in L^\infty(\Omega; \mathbb{R}^d)$; it introduces the reformulation of

the stray field energy contribution by the Helmholtz projection $\mathcal{P}$ as well as the penalty formulation for the side-restriction $|\mathbf{m}| \leq 1$; while this section continuous with the description of the discrete models, it ends with a review of a priori and a posteriori error control from [7]. Let $\mathbf{m} = (m_1, \ldots, m_d)$ be a magnetization and denote with $G : \mathbb{R}^d \backslash \{0\} \to \mathbb{R}$ the Newtonian kernel,

$$(2.1) \qquad G(x) := \begin{cases} -\gamma_2^{-1} \log |x| & \text{for } d = 2, \\ \gamma_d^{-1}/(d-2)\,|x|^{2-d} & \text{for } d > 2 \end{cases} \quad \text{for } x \neq 0,$$

where the positive constant γ_d is the surface measure of the unit sphere, e.g. $\gamma_2 = 2\pi$, $\gamma_3 = 4\pi$. With the convolution operator

$$(\mathcal{L}\mathbf{m})(x) := \sum_{j=1}^{d} (\partial G/\partial x_j * m_j)(x) \quad \text{for all } x \in \mathbb{R}^d$$

one can prove $u = \mathcal{L}\mathbf{m} \in H^1_{\ell oc}(\mathbb{R}^d)$, i.e. $u = \mathcal{L}\mathbf{m}$ has a weak derivative in $L^2(B(0,R))$ for any ball $B(0,R)$ around the origin 0 with arbitrary radius R. Moreover, one can show that $\nabla u = \nabla(\mathcal{L}\mathbf{m}) =: \mathcal{P}\mathbf{m}$ belongs to $L^2(\mathbb{R}^2, \mathbb{R}^2)$ and satisfies (1.5). The Helmholtz projection operator

$$\mathcal{P} : L^2(\mathbb{R}^d; \mathbb{R}^d) \to L^2(\mathbb{R}^d; \mathbb{R}^d)$$

is the L^2 orthogonal projection onto the linear and closed subspace of all the gradients [7, 17, 21, 22]. Hence, the stray field energy in $E_0^{**}(\mathbf{m})$ reads

$$\int_{\mathbb{R}^d} |\nabla u|^2 \, dx = \int_{\mathbb{R}^d} (\mathcal{P}\mathbf{m}) \cdot \mathbf{m} \, dx.$$

The Gâteaux derivative (also called first variation) of (RP) yields the Problem (P): Find $(\lambda, \mathbf{m}) \in L^2(\Omega) \times L^2(\Omega; \mathbb{R}^d)$ such that

$$(2.2) \qquad \mathcal{P}\mathbf{m} + D\phi^{**}(\mathbf{m}) + \lambda \mathbf{m} = \mathbf{f} \quad \text{a.e. in } \Omega,$$

$$(2.3) \qquad \lambda \geq 0, \ |\mathbf{m}| \leq 1, \ \lambda(1 - |\mathbf{m}|) = 0 \quad \text{a.e. in } \Omega.$$

The variable λ is the Lagrange multiplier for the side-restriction $|\mathbf{m}| \leq 1$ and (2.3) are the associated Kuhn-Tucker conditions. The term $\mathcal{P}\mathbf{m}$ from the stray field energy density is based on the projection property $\mathcal{P}^2 = \mathcal{P}$ and yields a problem (2.2) on the *bounded* magnetic domain Ω.

This problem (P) is well-posed in the sense that there exists a unique solution. Given a positive and small penalty parameter ε (possibly a given function of x in Ω) the penalization of (P) reads (P_ε): Find $\mathbf{m}_\varepsilon \in L^2(\Omega; \mathbb{R}^d)$ such that

$$(2.4) \qquad \mathcal{P}\mathbf{m}_\varepsilon + D\phi^{**}(\mathbf{m}_\varepsilon) + \lambda_\varepsilon \mathbf{m}_\varepsilon = f \quad \text{a.e. in } \Omega,$$

$$(2.5) \qquad \lambda_\varepsilon := \varepsilon^{-1} \max\{0, 1 - |\mathbf{m}_\varepsilon|^{-1}\} \quad \text{a.e. in } \Omega.$$

Problem (P_ε) is well-posed in the sense that there exists a unique solution. The spatial discretization of (P) and (P_ε) is based on a partition of Ω into a finite number of measurable subsets of Ω. Let $\mathcal{T}$ be a finite set of closed subsets of $\overline{\Omega}$ which are the closures $T = \overline{\text{int}(T)}$

of pairwise disjoint bounded Lipschitz domains $\operatorname{int}(T) \subset \Omega$. Then $\mathcal{L}^0(\mathcal{T})$ denotes the linear subspace of $\mathcal{T}$-piecewise constants, e.g. the mesh-size function

$$h := h_\mathcal{T} \in \mathcal{L}^0(\mathcal{T}) \subset L^\infty(\overline{\Omega}) \quad \text{defined by } h|_T := h_T := \operatorname{diam}(T) \text{ for all } T \in \mathcal{T}.$$

[Recall that $(\cdot)|_T$ denotes the restriction of a function $(\cdot)$ onto T.] Another example is $\mathbf{f}_h \in \mathcal{L}^0(\mathcal{T}; \mathbb{R}^d)$, the piecewise integral mean of the given right-hand side $\mathbf{f} \in L^2(\Omega; \mathbb{R}^d)$ defined by

$$\mathbf{f}_h|_T := |T|^{-1} \int_T f(x)\, dx \quad \text{for all } T \in \mathcal{T}.$$

Also, let $\varepsilon := \varepsilon_h \in \mathcal{L}^0(\mathcal{T})$ be a piecewise constant penalty parameter function. Then, a consistent Galerkin discretization of (P_ε) with $\mathcal{T}$-piecewise constant trial and test function reads $(P_{\varepsilon,h})$: Find $\mathbf{m}_h$ in $\mathcal{L}^0(\mathcal{T}; \mathbb{R}^d)$ such that

$$(2.6) \qquad |T|^{-1} \int_T (\mathcal{P}\mathbf{m}_h)(x)\, dx + D\phi^{**}(\mathbf{m}_h|_T) + \lambda_h|_T \mathbf{m}_h|_T = \mathbf{f}_h|_T \quad \text{for all } T \in \mathcal{T},$$

$$(2.7) \qquad \lambda_h|_T := (\varepsilon|_T)^{-1} \max\{0, 1 - |\mathbf{m}_h|_T|^{-1}\} \quad \text{for all } T \in \mathcal{T}.$$

The discrete model $(P_{\varepsilon,h})$ can be reformulated as a minimization problem to apply the direct method of the calculus of variations and to show the well-posedness, i.e. the unique existence of solutions. [If the elements $T \in \mathcal{T}$ are rectangular, it can be shown that the solution $(\lambda_h, \mathbf{m}_h)$ of $(RP_{\varepsilon,h})$ is unique (independent of ϕ^{**}), cf. Remark 2.5 of [7].]

The numerical solution of the unique solution $\mathbf{m}_h$ is the topic of the subsequent sections.

This section ends with a review of the a priori and a posteriori error analysis in [7] under the present notation. Throughout, let $(\lambda, \mathbf{m})$ and $(\lambda_h, \mathbf{m}_h)$ solve (P) and $(P_{\varepsilon,h})$ respectively. Then, there is an $\mathcal{T}$-independent constant $C > 0$ such that

$$\|\mathcal{P}\mathbf{m} - \mathcal{P}\mathbf{m}_h\|^2_{L^2(\mathbb{R}^d)} + \|D\phi^{**}(\mathbf{m}) - D\phi^{**}(\mathbf{m}_h)\|^2_{L^2(\Omega)} + \|\lambda\mathbf{m} - \lambda_h\mathbf{m}_h\|^2_{L^2(\Omega)}$$

$$(2.8) \qquad \leq C(1 + \|\varepsilon\|_{L^\infty(\Omega)}) \Big(\|\mathbf{m} - \mathbf{m}_\mathcal{T}\|^2_{L^2(\Omega)} + \|D\phi^{**}(\mathbf{m}) - (D\phi^{**}(\mathbf{m}))_\mathcal{T}\|^2_{L^2(\Omega)}$$

$$+ \|\lambda\mathbf{m} - (\lambda\mathbf{m})_\mathcal{T}\|^2_{L^2(\Omega)} \Big) + C\|\varepsilon\|_{L^\infty(\Omega)} \|\sqrt{\varepsilon}\, \lambda\mathbf{m}\|^2_{L^2(\Omega)}.$$

Here and below, $\mathbf{m}_\mathcal{T}$ (resp. $(D\phi^{**}(\mathbf{m}))_\mathcal{T}$) denotes the $\mathcal{T}$-piecewise integral mean of $\mathbf{m} \in L^\infty(\Omega; \mathbb{R}^d)$ (resp. $D\phi^{**}(\mathbf{m})$) and hence the first three terms on the right-hand side of (2.8) are best approximation errors. The last term $C\|\varepsilon\|_{L^\infty(\Omega)} \|\sqrt{\varepsilon}\lambda\mathbf{m}\|^2_{L^2(\Omega)}$ of order $O(\varepsilon^2)$ is the penalty error. If we suppose $\mathbf{m}$ and λ smooth (i.e. $\mathbf{m} \in H^1(\Omega; \mathbb{R}^d)$, $D\phi^{**}(\mathbf{m}) \in H^1(\Omega; \mathbb{R}^d)$, and $\lambda\mathbf{m} \in H^1(\Omega; \mathbb{R}^d)$) then (2.8) verifies

$$\|\mathcal{P}\mathbf{m} - \mathcal{P}\mathbf{m}_h\|_{L^2(\mathbb{R}^d)} + \|D\phi^{**}(\mathbf{m}) - D\phi^{**}(\mathbf{m}_h)\|_{L^2(\Omega)}$$

$$+ \|\lambda\mathbf{m} - \lambda_h\mathbf{m}_h\|_{L^2(\Omega)} + \|\sqrt{\varepsilon}\lambda_h\mathbf{m}_h\|_{L^2(\Omega)} = O(\varepsilon + h).$$

In the same spirit, there holds an a posteriori error estimate

$$\|\mathcal{P}\mathbf{m} - \mathcal{P}\mathbf{m}_h\|^2_{L^2(\mathbb{R}^d)} + \|D\phi^{**}(\mathbf{m}) - D\phi^{**}(\mathbf{m}_h)\|^2_{L^2(\Omega)}$$

$$(2.9) \qquad \leq 2 \big\{ \|\varepsilon\, \lambda_h\mathbf{m}_h\|^2_{L^2(\Omega)} + \|\varepsilon|\lambda_h\mathbf{m}_h|\{(\mathbf{f} - \mathbf{f}_h) - (\mathcal{P}\mathbf{m}_h - (\mathcal{P}\mathbf{m}_h)_\mathcal{T})\}\|_{L^1(\Omega)}$$

$$+ \langle(\mathbf{f} - \mathbf{f}_h) - (\mathcal{P}\mathbf{m}_h - (\mathcal{P}\mathbf{m}_h)_\mathcal{T}) ; \mathbf{m} - \mathbf{m}_\mathcal{T}\rangle_{L^2(\Omega)} \big\}.$$

The right-hand side of (2.9) is not fully computable as it contains $\mathbf{m} - \mathbf{m}_\mathcal{T}$. Since $|\mathbf{m}| \leq 1$ there follows $\|\mathbf{m} - \mathbf{m}_\mathcal{T}\|_{L^\infty(\Omega)} \leq 1$ and, hence, by Hölder's inequality

$$\langle (\mathbf{f} - \mathbf{f}_\mathcal{T}) - (\mathcal{P}\mathbf{m}_h - (\mathcal{P}\mathbf{m}_h)_\mathcal{T}) \, ; \, \mathbf{m} - \mathbf{m}_\mathcal{T} \rangle_{L^2(\Omega)} \leq 2\|(\mathbf{f} - \mathbf{f}_\mathcal{T}) - (\mathcal{P}\mathbf{m}_h - (\mathcal{P}\mathbf{m}_h)_\mathcal{T})\|_{L^1(\Omega)}.$$

For $\mathbf{m} \in W^{1,\infty}(\Omega; \mathbb{R}^d)$, the Poincaré estimate leads to

$$\langle (\mathbf{f} - \mathbf{f}_\mathcal{T}) - (\mathcal{P}\mathbf{m}_h - (\mathcal{P}\mathbf{m}_h)_\mathcal{T}) \, ; \, \mathbf{m} - \mathbf{m}_\mathcal{T} \rangle_{L^2(\Omega)} \leq C \, \|h\{(\mathbf{f} - \mathbf{f}_\mathcal{T}) - (\mathcal{P}\mathbf{m}_h - (\mathcal{P}\mathbf{m}_h)_\mathcal{T})\}\|_{L^1(\Omega)}$$

with a constant $C = C_P \|\mathbf{m}\|_{W^{1,\infty}(\Omega)}$.

The two resulting a posteriori error estimates are reliable (in the first case as no assumption on the smoothness of the unknown solution $\mathbf{m}$ is included) but not efficient (as the estimate behaves too coarse - cf. [7] and the numerical examples below); or, conversely, efficient (as the second estimate shows the higher convergence rates) but *not* reliable (or it appears doubtful to assume a higher smoothness like $\mathbf{m} \in W^{1,\infty}(\Omega; \mathbb{R}^d)$). This phenomenon is called reliability-efficiency gap in [5]: What is reliable is not efficient and what is efficient is not reliable. The reason is a lack of control over the term $\|\mathbf{m} - \mathbf{m}_h\|_{L^2(\Omega)}$. The estimates allow control over $\|\mathbf{z}_j \cdot (\mathbf{m} - \mathbf{m}_h)\|_{L^2(\Omega)}$ for $j = 2, 3, \ldots, d$ via $\|D\phi^{**}(\mathbf{m}) - D\phi^{**}(\mathbf{m}_h)\|_{L^2(\Omega)}$ but not over $\|\mathbf{e} \cdot (\mathbf{m} - \mathbf{m}_h)\|_{L^2(\Omega)}$ and so we lack any improved estimate over $\|\mathbf{m} - \mathbf{m}_\mathcal{T}\|_{L^2(\Omega)} \leq \|\mathbf{m} - \mathbf{m}_h\|_{L^2(\Omega)}$.

3. Numerical Algorithms

This section presents the details on the numerical algorithms with emphasis on the Newton-Raphson solver. Since there is a small penalty parameter involved, the performance of the documented schemes will be studied in the subsequent sections. The discrete equations with respect to a triangulation $\mathcal{T} = \{T_1, \ldots, T_N\}$ lead to the unknown coefficients $\mathbf{x} \in \mathbb{R}^{dN}$ of

$$(3.1) \qquad \mathbf{m}_h = \sum_{j=1}^{N} \sum_{\alpha=1}^{d} \mathbf{x}_{[j,\alpha]} \varphi_{[j,\alpha]} \in L^\infty(\Omega; \mathbb{R}^d).$$

Here, one abbreviates $[j, 1] := j$ and $[j, 2] := j + N$ in 2D (and furthermore $[j, 3] := j + 2N$ for 3D) to fix the order of the coefficients and $\varphi_{[j,\alpha]} := \chi_{T_j} \mathbf{e}_\alpha$ is the vector valued function with the value $(\delta_{1\alpha}, \ldots, \delta_{d\alpha})$ [i.e. the k-th canonical unit vector for Kronecker's $\delta_{\alpha\beta}$] on T_j which vanishes outside T_j. In terms of the coefficients (3.1) and with the abbreviate notation $\varepsilon_k := \varepsilon|_{T_k}$ and $\mathbf{x}^{(k)} := (\mathbf{x}_{[k,1]}, \ldots, \mathbf{x}_{[k,d]}) \in \mathbb{R}^d$, the discrete problem $(P_{\varepsilon,h})$ reads

$$|T_k|^{-1} \sum_{j=1}^{N} \sum_{\alpha=1}^{d} \int_{T_k} (\mathcal{P}\varphi_{[j,\alpha]}) \, dx + \varepsilon_k^{-1} \max\{0, 1 - |\mathbf{x}^{(k)}|^{-1}\} \mathbf{x}^{(k)} + D\phi^{**}(\mathbf{x}^{(k)}) - \mathbf{f}_h|_{T_k} = 0 \in \mathbb{R}^d$$

for all $k = 1, 2, \ldots, N$. This nonlinear system of equations is recast as

$$\mathbf{F}(\mathbf{x}) = 0 \in \mathbb{R}^{dN}$$

and then solved by the Newton-Raphson scheme. The following termination criterion is based on suggestions in [15].

Algorithm 3.1 (Newton-Raphson). ***Input:*** *Let* $\mathbf{x}^{(0)} \in \mathbb{R}^{dN}$ *be a given initial vector.*
(i) *Call Newton-Rhapson scheme to compute* $\mathbf{x}^{(1)}, \ldots, \mathbf{x}^{(k)} \in \mathbb{R}^{dN}$ *until*

$$|\mathbf{F}(\mathbf{x}^{(k)})| \leq 10^{-12} + 10^{-6}|\mathbf{F}(\mathbf{x}^{(0)})| \quad or \quad k = 100.$$

(ii) *In case $k = 100$ stop with an error message. Otherwise call Newton-Rhapson scheme with initial vector $\mathbf{x}^{(k)}$ to compute $\mathbf{x}^{(k+1)}, \ldots, \mathbf{x}^{(\ell+1)} \in \mathbb{R}^{dN}$ until*

$$|\mathbf{F}(\mathbf{x}^{(\ell)})| \leq \min\{10^{-12}, |\mathbf{F}(\mathbf{x}^{(\ell+1)})|\} \quad or \quad \ell = 100.$$

(iii) *In case $\ell = 100$ stop with an error message. Otherwise $\mathbf{x}^{(\ell)}$ is an approximation of the (unique) zero of $\mathbf{F}$.*
Output: *Either error message or the number ℓ of iterations and $\mathbf{x} := \mathbf{x}^{(\ell)}$ as an approximation to the zero of $\mathbf{F}$.*

The evaluation of $\mathbf{F}(\mathbf{x})$ and $D\mathbf{F}(\mathbf{x})$ is possible with a closed form formulae for the stiffness matrix $\mathbf{A}$ of the operator $\mathcal{P}$ from [7, 21]. The following algorithm is formulated for $2D$ but works for $3D$ analogously. In particular, it shows that $\mathbf{F}(\mathbf{x})$ and $D\mathbf{F}(\mathbf{x})$ can be assembled in linear complexity up to one matrix-vector multiplication.

Algorithm 3.2 (Compute $\mathbf{F}(\mathbf{x})$ and $D\mathbf{F}(\mathbf{x})$). ***Input:*** $\mathbf{x} \in \mathbb{R}^{2N}$, $\mathbf{A} \in \mathbb{R}^{2N \times 2N}_{sym}$ *defined by* $\mathbf{A}_{[j,\alpha][k,\beta]} := \int_{T_j} (\mathcal{P}\varphi_{[k,\beta]}) \cdot \varphi_{[j,\alpha]} \, dx$ *and* $\mathbf{z} \in \mathbb{R}^2$ *such that* $D\phi^{**}(x) = (x \cdot \mathbf{z})\mathbf{z}$ *for all* $x \in \mathbb{R}^2$ *and set* $\mathbf{b} := \mathbf{Ax}$; $\mathbf{M} := \mathbf{A}$;.
Compute:

```
for j = 1 to N
    mhT= (x_[j,1], x_[j,2])^T ∈ ℝ²;
    (b_[j,1], b_[j,2])^T := (b_[j,1], b_[j,2])^T + |T_j|(mhT · z) z − ∫_{T_j} f dx;
    ( M^11_jj  M^12_jj ) := ( M^11_jj  M^12_jj ) + |T_j| z ⊗ z;
    ( M^21_jj  M^22_jj )    ( M^21_jj  M^22_jj )
    if ℓ := |mhT| > 1
        (b_[j,1], b_[j,2])^T := (b_[j,1], b_[j,2])^T + ε_j^{-1}|T_j|(1 − ℓ^{-1}) mhT;
        ( M^11_jj  M^12_jj ) := ( M^11_jj  M^12_jj ) + ε_j^{-1}|T_j|{ (1 − ℓ^{-1})( 1  0 ) + ℓ^{-3} mhT ⊗ mhT };
        ( M^21_jj  M^22_jj )    ( M^21_jj  M^22_jj )                            ( 0  1 )
    endif
endfor.
```

Output: $D\mathbf{F}(\mathbf{x}) = \mathbf{M} \in \mathbb{R}^{2N \times 2N}_{sym}$ *and* $\mathbf{F}(\mathbf{x}) = \mathbf{b} \in \mathbb{R}^{2N}$.

The rectangular elements employed throughout this paper guarantee that $D\mathbf{F}(\mathbf{x})$ is always positive definite. Our calculations confirmed this in the sense that they did not show any instabilities.

The nested Newton-Raphson solver in Algorithm 3.1 is part of a multilevel scheme driven by an adaptive algorithm. As in [7], we adopted the estimators

$$(3.2) \qquad \mu := \left(\sum_{T \in \mathcal{T}} \mu_T^2 \right)^{1/2} \qquad \text{and} \qquad \eta := \left(\sum_{T \in \mathcal{T}} \eta_T^2 \right)^{1/2}$$

with the refinement indicators μ_T, η_T, for $T \in \mathcal{T}$, defined by

$$\ell_T := (\varepsilon\lambda_h|\mathbf{m}_h|)|_T = \max\{0, |\mathbf{m}_h|_T| - 1\},$$
$$(3.3) \qquad \mu_T^2 := (1 + \ell_T)\|(\mathbf{f} - \mathbf{f}_{\mathcal{T}}) - (\mathcal{P}\mathbf{m}_h - (\mathcal{P}\mathbf{m}_h)_{\mathcal{T}})\|_{L^1(T)} + |T|\ell_T^2,$$
$$\eta_T^2 := (h_T + \ell_T)\|(\mathbf{f} - \mathbf{f}_{\mathcal{T}}) - (\mathcal{P}\mathbf{m}_h - (\mathcal{P}\mathbf{m}_h)_{\mathcal{T}})\|_{L^1(T)} + |T|\ell_T^2.$$

The estimator μ is reliable, i.e. an upper bound for the error $\|\mathcal{P}\mathbf{m} - \mathcal{P}\mathbf{m}_h\|_{L^2(\mathbb{R}^d)} + \|D\phi^{**}(\mathbf{m}) - D\phi^{**}(\mathbf{m}_h)\|_{L^2(\Omega)}$ up to a multiplicative constant, but cannot be efficient; the estimator η is reliable solely for $\mathbf{m} \in W^{1,\infty}(\Omega; \mathbb{R}^d)$, but expected to be efficient.

Algorithm 3.3 (Adaptive Mesh-Refinement). ***Input:*** *Initial triangulation* $\mathcal{T}^{(0)}$, $\alpha > 0$, *and* $0 \leq \theta \leq 1$. *Set* $n = 0$ *and* $\mathbf{m}_h := 0$.
Compute for $n = 1, 2, \ldots$ *until termination*
(i) *On* $T_j \in \mathcal{T}^{(n)} = \{T_1, \ldots, T_N\}$ *set* $\varepsilon|_{T_j} := \varepsilon_j = h_{T_j}^\alpha > 0$, $j = 1, \ldots, N$
(ii) *Call Algorithm 3.1 with start vector associated to* $\mathbf{m}_h^{(n-1)}$ *and output* $\mathbf{m}_h^{(n)}$.
(iii) *Compute* μ *and* η *from* (3.2) *and indicators* $\eta_j := \eta_{T_j}$ *and* $\mu_j := \mu_{T_j}$ *from* (3.3) *with* $\mathbf{m}_h$ *substituted by* $\mathbf{m}_h^{(n)}$.
(iv) *Mark an element* $T_j \in \mathcal{T}^{(n)}$ *provided* $\eta_j \geq \theta \max_{1 \leq k \leq N} \eta_k$ *(or* μ_j *respectively)*.
(v) *Refine the marked elements, update* n *and go to* (i).
Output: *Sequence of* $\mathcal{T}^{(n)}$, $\eta^{(n)}$, $\mu^{(n)}$, $\mathbf{m}_h^{(n)}$ *for* $n = 1, 2, \ldots,$.

The choice $\theta = 0$ in Algorithm 3.3 leads to uniform mesh-refinement, whereas $\theta = 1/2$ leads to adapted meshes. The remaining implementational details (on the calculations of $\mathbf{A}$, η_j, μ_j and the mesh-design in quads) will be given in [7].

This section will be concluded with a few remarks on the fast (approximate) evaluation of the stiffness matrix $\mathbf{A}$ of Algorithm 3.2 for the nonlocal operator $\mathcal{P}$; further details on this $\mathcal{H}^2$-matrix approach will appear in [23]. Given two elements T_j and T_k with (large) positive distance, the entry

$$\mathbf{A}_{[j,\alpha],[k,\beta]} = \int_{T_j} \int_{T_k} \frac{\partial^2 G}{\partial x_\alpha \partial x_\beta}(x - y) \, dy \, dx \quad \text{for } 1 \leq j, k \leq N \text{ and } 1 \leq \alpha, \beta \leq d$$

is approximated by replacing the (smooth) integral kernel

$$g_{\alpha\beta}(x, y) = \frac{\partial^2 G}{\partial x_\alpha \partial x_\beta}(x - y) \quad \text{for } \alpha, \beta = 1, 2, \ldots, d$$

by a tensor product of polynomials in x and y. For certain sets of elements $\sigma, \tau \subseteq \mathcal{T}$ and associated domains $\cup\sigma$ resp. $\cup\tau$ with large distance (obtained by a cluster tree partitioning of $\mathcal{T}$, cf. [2]), let vectors $x_{m_1}^{(\sigma)} \in \cup\sigma$, $y_{m_2}^{(\tau)} \in \cup\tau$ and polynomials $p_{m_1}^{(\sigma)}, p_{m_2}^{(\tau)}$ on $\cup\sigma$ resp. $\cup\tau$ be given and define

$$\tilde{g}_{\alpha\beta}(x, y) := \sum_{m_1=1}^{M_1} \sum_{m_2=1}^{M_2} g_{\alpha\beta}(x_m^{(\sigma)}, y_{m_2}^{(\tau)}) \, p_{m_1}^{(\sigma)}(x) \, p_{m_2}^{(\tau)}(y) \quad \text{for } x \in \cup\sigma \text{ and } y \in \cup\tau.$$

Given any $T_j \in \sigma$ and $T_k \in \tau$ the fast approximate evaluation of the submatrix $\mathbf{A}^{\alpha\beta}|_{\sigma \times \tau}$ of $\mathbf{A}^{\alpha\beta} \in \mathbb{R}_{sym}^{N \times N}$, $\mathbf{A}_{jk}^{\alpha\beta} := \mathbf{A}_{[j,\alpha],[k,\beta]}$, is based on the approximation

$$\mathbf{A}_{[j,\alpha],[k,\beta]} \approx \sum_{m_1=1}^{M_1} \sum_{m_2=1}^{M_2} g_{\alpha\beta}(x_{m_1}^{(\sigma)}, y_{m_2}^{(\tau)}) \left\{ \int_{T_j} p_{m_1}^{(\sigma)}(x) \, dx \right\} \left\{ \int_{T_k} p_{m_2}^{(\tau)}(y) \, dy \right\}.$$

It is shown in [25, 19] for other integral kernels that storage and matrix-vector multiplication with $\mathcal{H}^2$-matrix are of linear complexity $O(N)$ instead of $O(N^2)$. Finally, the $\mathcal{H}$-matrix approach can also be employed for a fast evaluation of the refinement indicators [21, 23].

4. NUMERICAL EXPERIMENTS WITH KNOWN EXACT SOLUTION

This section presents some numerical results obtained with the multilevel adaptive solver of Section 3. The example is adopted from [7] to study the performance of the solver.

The unit square $\Omega = (0,1)^2$ is filled with a uniaxial magnetic material (1.4) with easy axis $\mathbf{e} = (-1,1)/\sqrt{2}$ and $\mathbf{z} = (1,1)/\sqrt{2}$. Then,

$$(4.1) \qquad (\mathbf{m}(x), \lambda(x)) := \begin{cases} (\mathbf{y}(x), 0) & \text{for } x \in \omega, \\ (x_1 x_2 (1 - y_1(x))^{-1}(1 - y_2(x))^{-2}\mathbf{y}(x), 1) & \text{for } x \in \Omega \backslash \omega \end{cases}$$

PSfrag replacements
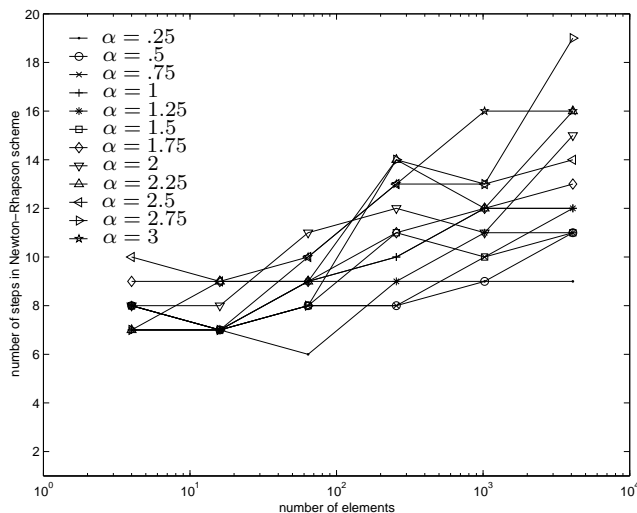
FIGURE 4.1. Convergence history for uniform mesh-refinement ($\theta = 0$) on performance of the Newton-Raphson scheme for different choices of the penalization parameter $\varepsilon = h^\alpha$ with $\alpha = 0.25, \ldots, 3$. The number of iteration steps in Algorithm 3.1 depends only slightly on α and is plotted as a function of N.

defines the solution with a singular gradient at the three vertices $(0,1)$, $(1,0)$, $(1,1)$ on the boundary of the magnetic body $\Omega = (0,1)^2$ with given right-hand side

$$(4.2) \qquad \mathbf{f} := \mathcal{P}\mathbf{m} + (\mathbf{m} \cdot \mathbf{z})\mathbf{z} + \lambda\mathbf{m} \in L^2(\Omega; \mathbb{R}^2).$$

Here,

$$\mathbf{y}(x) := \frac{(1,1) - x}{|(1,1) - x|} \quad \text{and} \quad \omega := \left\{ x \in \Omega \, \middle| \, |(1,1) - x| < 1 \right\}.$$

The adapted meshes and several conclusions on the reliability - efficiency gap are drawn in [7] and hence not repeated here. The convergence history for Algorithm 3.1 is depicted in Figure 4.1 for uniform mesh-refining and Figure 4.2 for adaptive mesh-refining. In both cases, the number of iteration increases moderately with the number of unknowns in the multilevel meshed iteration. The smaller the parameter α the larger is the discretization error discussed in [7] but the smaller is the computational effect displayed in Figure 4.1. Since the difference is not too large, we omitted a refined strategy which begins with a moderate α and eventually increases α from level to level. In fact, it seems that the choice
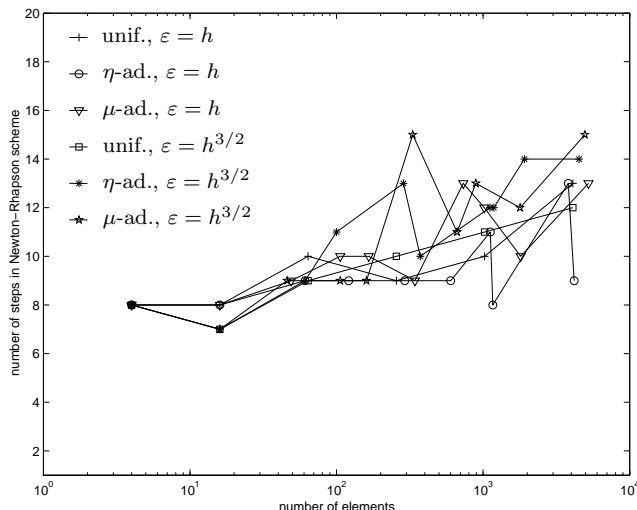
PSfrag replacements

FIGURE 4.2. Convergence history for uniform mesh-refinement ($\theta = 0$) on performance of the Newton-Raphson scheme for adaptive mesh-refinement $\theta = 1/2$ and penalization with $\varepsilon = h$ and $\varepsilon = h^{3/2}$. The number of iteration steps in Algorithm 3.1 depends only slightly on α and N, although the meshes are highly adapted. Moreover, the figure shows the number of steps for the corresponding uniform mesh-refinement for comparison. The increase of the computational cost with N for adaptive mesh-refinement compares with that for uniform mesh-refinement.

$\alpha = 3/2$ already proposed in [7] yields a fair compromise with $k < 20$ iteration steps for each level.

5. NUMERICAL EXAMPLE ON A PRACTICAL APPLICATION

The final set of examples concern the ferromagnetic beam $\Omega = (-1/2, 1/2) \times (-5/2, 5/2)$ [8] with easy axis $\mathbf{e} = (1, 0)$ loaded with three different loads $\mathbf{f}^{(1)} = (6, 0)$ parallel, $\mathbf{f}^{(2)} = (0.5, 0.5)$ diagonally, and $\mathbf{f}^{(3)} = (0, 0.9)$ orthogonal to the easy axis. Figure 5.1 displays the effective magnetization vectors and their lengths in a grey scale computed with $\theta = 0$ in Algorithm 3.3 on $\mathcal{T}^{(3)}$. We observe some moderate changes of the orientation near the vertices of Ω and hence run Algorithm 3.3 with $\theta = 1/2$ for η-adapted meshes shown in the respective Figure 5.10, 5.11, and 5.12. Therein, the magnetic potential $\mathcal{L}\mathbf{m}_h$ is displayed as well on a neighbourhood of Ω. It is stressed that the isolines indicate the fact that the approximation is in the entire space $\mathbb{R}^2$ and not restricted to a bounded subset as in [8]. The discretization history of the meshes and a picture of the approximation of λ_h are given in Figure 5.2 and Figure 5.3 for $\mathbf{f}^{(1)}$, in Figure 5.4 and Figure 5.5 for $\mathbf{f}^{(2)}$, and in Figure 5.6 and Figure 5.7 for $\mathbf{f}^{(3)}$. In contrast to the FE model in [8] and as quite some surprise to us [7], there is a moderate refinement towards the vertices only. Figure 5.8 shows the empirical convergence history and (as the true effective magnetization is unknown) plots the estimators μ and η as functions of N for uniform and adaptive mesh-refinements. It turns out that, in fact, adaptive refinements - although superior - are not really necessary here [7]. The convergence history of the Newton-Rhapson scheme for $\varepsilon = h$ and $h^{3/2}$ in Figure 5.9 is similar to the previous example and so proves that our proposed adaptive multilevel scheme
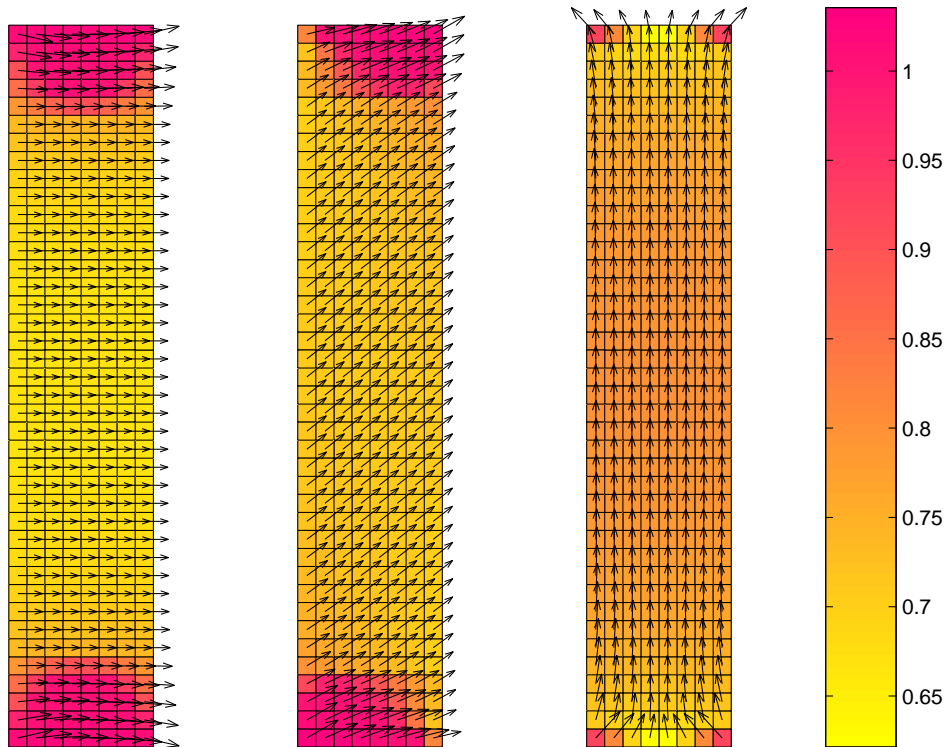
FIGURE 5.1. Discrete magnetizations $\mathbf{m}_h$ in Section 5 for $\mathbf{f}^{(1)}$, $\mathbf{f}^{(2)}$, and $\mathbf{f}^{(3)}$ (from left to right) and penalization with $\varepsilon = h^{3/2}$ on a uniform mesh $\mathcal{T}_3$ with $N = 320$ elements.

of Algorithm 3.3 with a meshed Newton-Raphson scheme performs well for real-life scientific computing.

6. CONCLUSIONS

The final section presents conclusions, comments, and remarks on future developments.

6.1. **Resume.** In the large and soft body limit of micromagnetics, the effective magnetization vector, i.e. the space average of the micromagnetic magnetization vectors, can be calculated directly from an effective model (P). Therein, exterior field problem can be recast via some Helmholtz projection operator $\mathcal{P}$ that allows a nonlocal problem for L^∞ functions on the magnetic domain Ω. The convexified pointwise side-restriction $|\mathbf{m}| \leq 1$ can be involved in a penalization problem (P_ε). The associated discrete problem $(P_{\varepsilon,h})$ acts on piecewise constant trial and test functions. The work [7] presented a throughout a priori and a posteriori error analysis of the discretization errors.

This paper presented an adaptive multilevel scheme with a nested Newton-Raphson iteration for the efficient solution of the discrete effective model. The numerical experiments of this paper illustrate the almost linear complexity of the scheme. Although a direct solver is employed here, an iterative scheme for the linear subproblems might easily be involved and
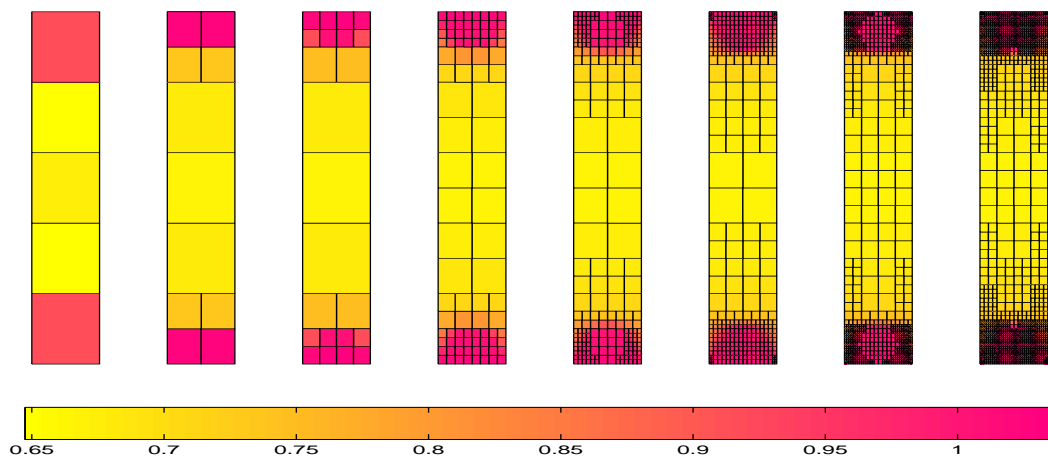
FIGURE 5.2. η-adaptively generated meshes $\mathcal{T}_0$ (with $N = 5$) till $\mathcal{T}_7$ (with $N = 1604$) in Section 5 for $\mathbf{f}^{(1)} = (.6, 0)$, $\mathbf{e} = (1, 0)$, and $\varepsilon = h^{3/2}$. The grey scale shows the length $|\mathbf{m}_h|$ of the discrete solution.
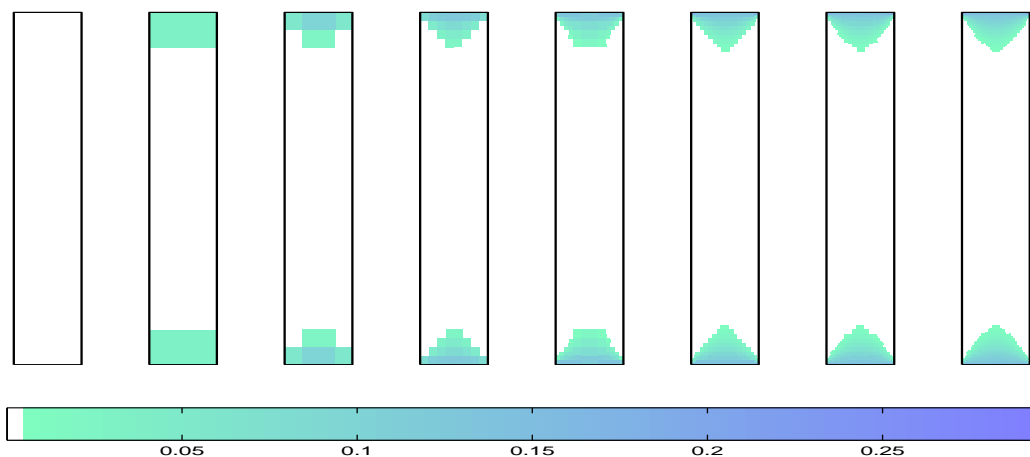

FIGURE 5.3. Discrete Lagrange multiplier λ_h on η-adaptively generated meshes $\mathcal{T}_0$ (with $N = 5$) till $\mathcal{T}_7$ (with $N = 1604$) in Section 5 for $\mathbf{f}^{(1)} = (.6, 0)$, $\mathbf{e} = (1, 0)$, and $\varepsilon = h^{3/2}$. The grey scale shows the pointwise value of λ_h. In the white region we have $\lambda_h \equiv 0$, i.e. $|\mathbf{m}_h| \leq 1$.

is supported by an $\mathcal{H}$-matrix approach [23]. The overall empirical experience of this paper and that of [7] supports the subsequent remarks.

6.2. **Effective Modelling of Effective Magnetization.** The model $(P_{\varepsilon,h})$ allows the efficient simulation of the effective magnetization vectors. This yields a macroscopic approximation of a multi-scale problem with a complicated microscopic structure which would be
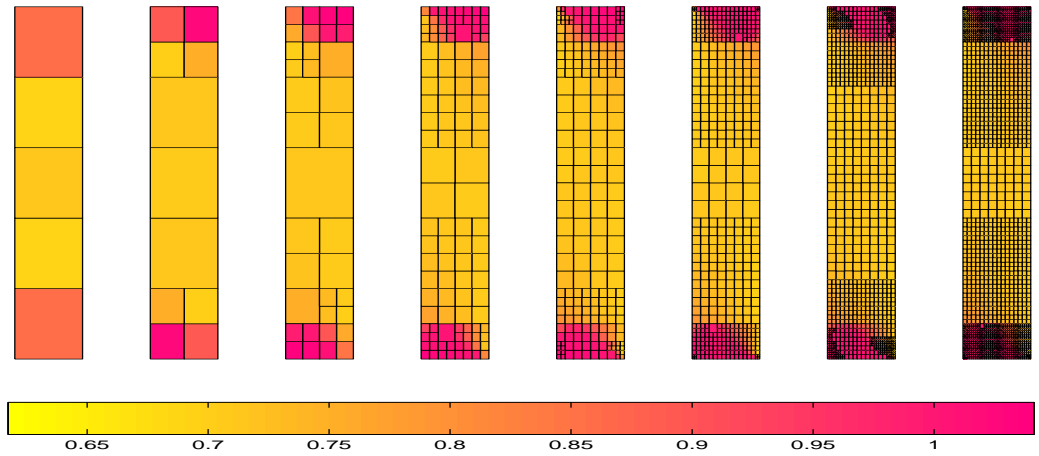
FIGURE 5.4. η-adaptively generated meshes $\mathcal{T}_0$ (with $N = 5$) till $\mathcal{T}_7$ (with $N = 1886$) in Section 5 for $\mathbf{f}^{(2)} = (.5, 5)$, $\mathbf{e} = (1, 0)$, and $\varepsilon = h^{3/2}$. The grey scale shows the length $|\mathbf{m}_h|$ of the discrete solution.
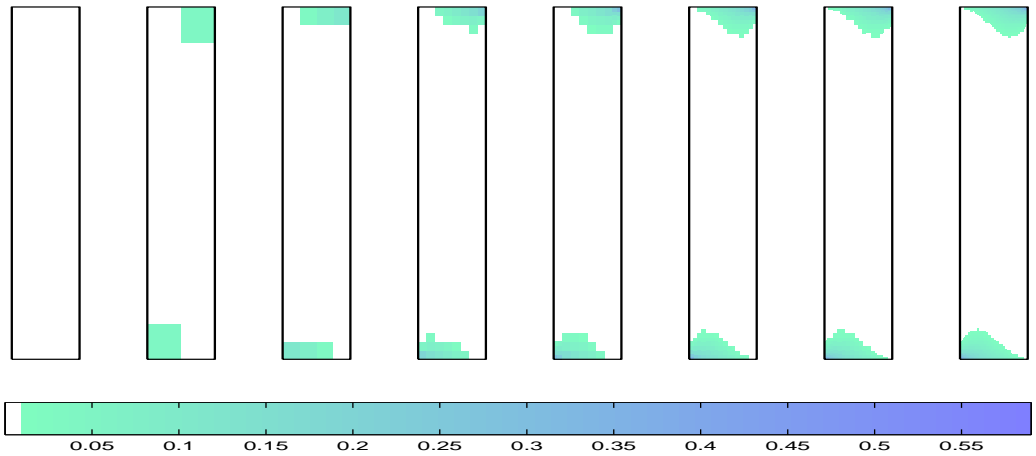

FIGURE 5.5. Discrete Lagrange multiplier λ_h on η-adaptively generated meshes $\mathcal{T}_0$ (with $N = 5$) till $\mathcal{T}_7$ (with $N = 1886$) in Section 5 for $\mathbf{f}^{(2)} = (.5, .5)$, $\mathbf{e} = (1, 0)$, and $\varepsilon = h^{3/2}$. The grey scale shows the pointwise value of λ_h. In the white region we have $\lambda_h \equiv 0$, i.e. $|\mathbf{m}_h| \leq 1$.

impossible to compute by a resolution of the fines scale phenomena. We refer to [4] for a one-dimensional trivial example of non-convex minimization problem that illustrates that cluster of local minimizers in the high-dimensional global non-convex minimization problem yield an extremely difficult discrete problem one should not assume to be able to solve accurately.

6.3. Competition with [8]**.** The adaptive mesh-refinements can be very important to improve the empirical convergence rates. In many cases, however, the improvements in accuracy
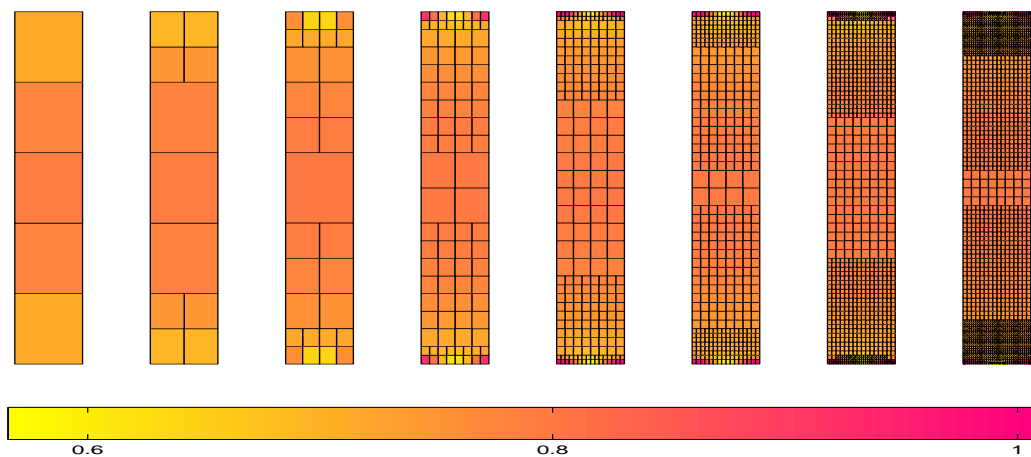
FIGURE 5.6. η-adaptively generated meshes $\mathcal{T}_0$ (with $N = 5$) till $\mathcal{T}_7$ (with $N = 2216$) in Section 5 for $\mathbf{f}^{(3)} = (0, .9)$, $\mathbf{e} = (1, 0)$, and $\varepsilon = h^{3/2}$. The grey scale shows the length $|\mathbf{m}_h|$ of the discrete solution.
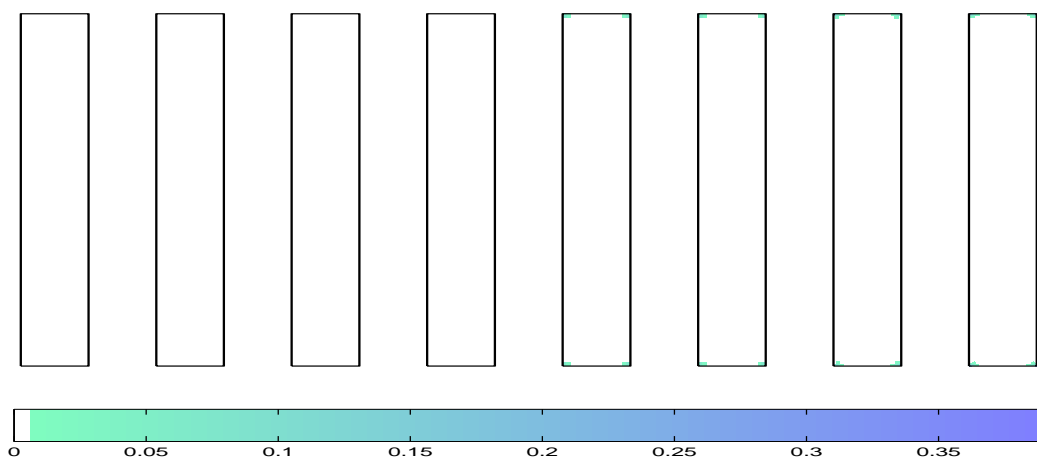

FIGURE 5.7. Discrete Lagrange multiplier λ_h on η-adaptively generated meshes $\mathcal{T}_0$ (with $N = 5$) till $\mathcal{T}_7$ (with $N = 2216$) in Section 5 for $\mathbf{f}^{(3)} = (0, .9)$, $\mathbf{e} = (1, 0)$, and $\varepsilon = h^{3/2}$. The grey scale shows the pointwise value of λ_h. In the white region we have $\lambda_h \equiv 0$, i.e. $|\mathbf{m}_h| \leq 1$. Except on the vertices, we see that there is almost no penalization.

the discrete model $(P_{\varepsilon,h})$ do not really require a local mesh-refining. This is in contrast to the discrete model of [8] where every vertex of the domain Ω yielded a local mesh-refinement towards it. In this sense, the presented Algorithm 3 is superior to the suggested schemes of [8]. This is particularly true for the accuracy of the magnetic potential $u := \mathcal{L}\mathbf{m}$ which is a macroscopic quantity (e.g. it is smooth and does not exhibit oscillations) in the exterior unbounded domain. This point is modelled exactly in $(P_{\varepsilon,h})$ while the truncation error of a
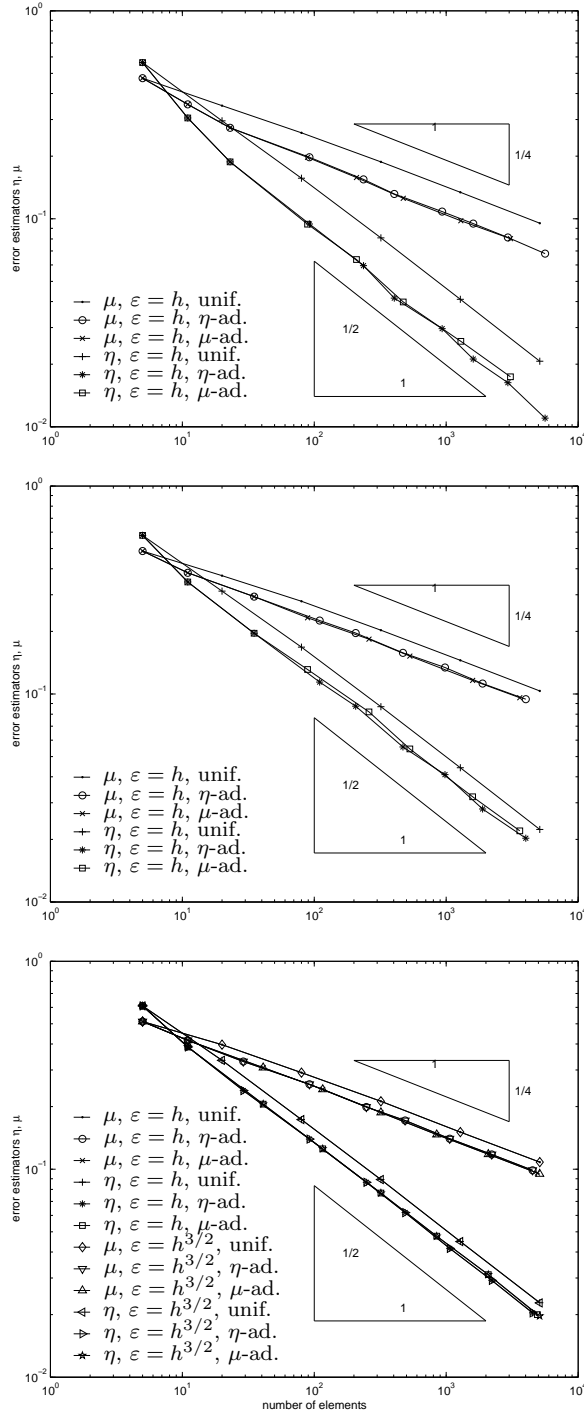
PSfrag replacements

μ, $\varepsilon = h^{3/2}$, unif.

μ, $\varepsilon = h^{3/2}$, η-ad.

μ, $\varepsilon = h^{3/2}$, μ-ad.

η, $\varepsilon = h^{3/2}$, unif.

η, $\varepsilon = h^{3/2}$, η-ad.

η, $\varepsilon = h^{3/2}$, μ-ad.

PSfrag replacements

μ, $\varepsilon = h^{3/2}$, unif.

μ, $\varepsilon = h^{3/2}$, η-ad.

μ, $\varepsilon = h^{3/2}$, μ-ad.

η, $\varepsilon = h^{3/2}$, unif.

η, $\varepsilon = h^{3/2}$, η-ad.

η, $\varepsilon = h^{3/2}$, μ-ad.

PSfrag replacements

FIGURE 5.8. Experimental convergence of the error estimators η and μ in Section 5 for $\mathbf{f}^{(1)}$, $\mathbf{f}^{(2)}$, and $\mathbf{f}^{(3)}$ (from top to bottom) and uniform, η-adaptive, and μ-adaptive mesh-refinement corresponding to the penalization parameter $\varepsilon = h^{3/2}$. There is (up to a multiplicative constant) no improvement of the convergence behaviour by the adaptive mesh-refining strategies, although we observe some local mesh-refinement towards the corners for $\mathbf{f}^{(1)}$ and $\mathbf{f}^{(2)}$, cf. Figure 5.2 and 5.4.

PSfrag replacements

PSfrag replacements
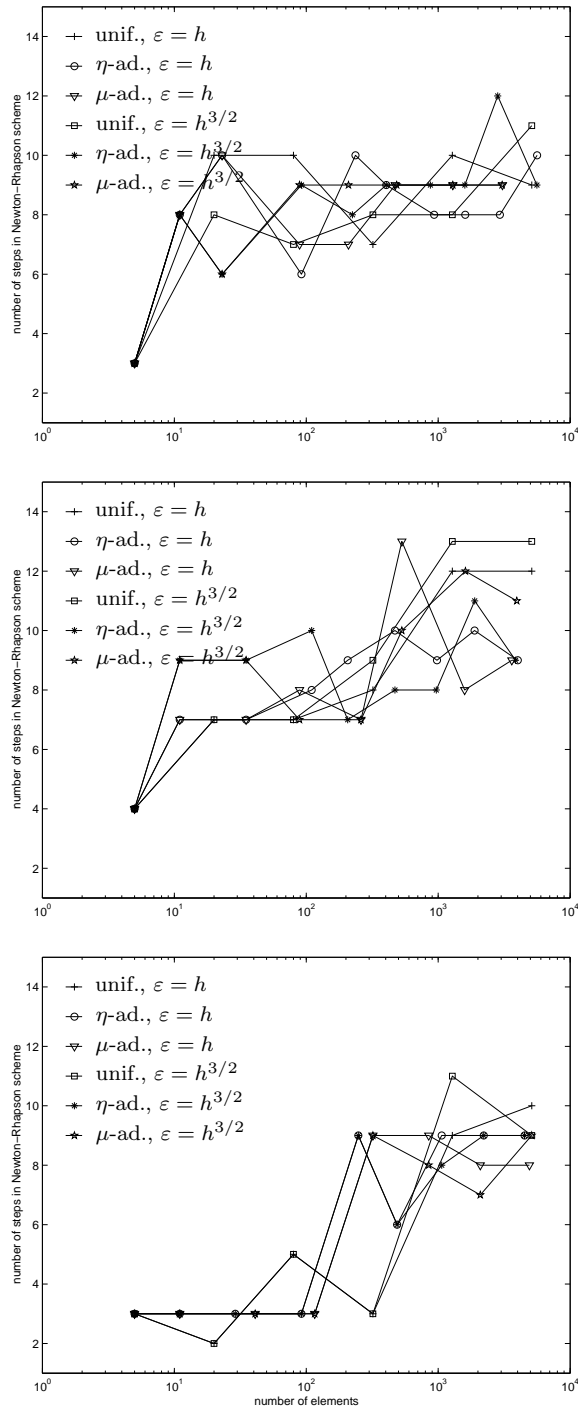
PSfrag replacements

FIGURE 5.9. Convergence history for uniform mesh-refinement ($\theta = 0$) on performance of the Newton-Raphson scheme for adapted mesh-refinement and penalization with $\varepsilon = h$ and $\varepsilon = h^{3/2}$ for $\mathbf{f}^{(1)}$, $\mathbf{f}^{(2)}$, and $\mathbf{f}^{(3)}$ (from top to bottom). The number of iteration steps in Algorithm 3.1 depends only slightly on α and N.
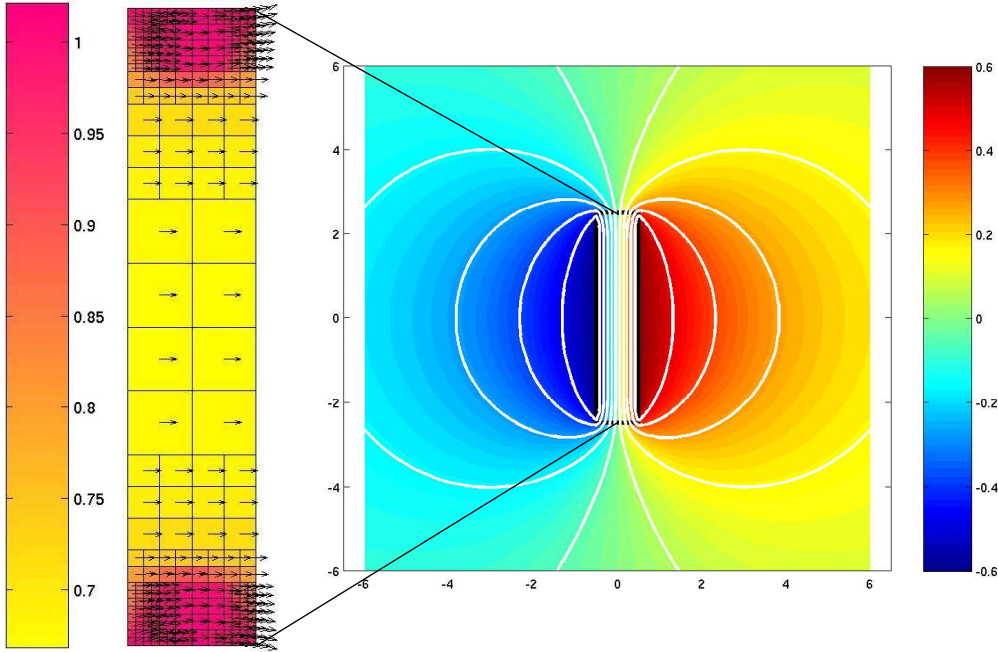
FIGURE 5.10. Discrete Magnetization $\mathbf{m}_h$ (zoom on the left) on the η-adaptively generated mesh $\mathcal{T}_4$ (with $N = 236$) and corresponding potential u_h (right) for constant exterior field $\mathbf{f}^{(1)} = (.6, 0)$ and penalization parameter $\varepsilon = h^{3/2}$. The grey scale in the zoomed magnet displays the length $|\mathbf{m}_h|$ of the discrete magnetization. On the right, the pointwise value of u_h is shown by grey scale and some isolines have been drawn.

bounded neighbourhood $\hat{\Omega}$ of the magnetic body is NOT included in the analysis of [8] (for simplicity).

6.4. Fast Evaluation of Integral Operator. Comparing the CPU times, the $\mathcal{H}$-matrix approach yields a fast evaluation in Algorithm 2 and then is comparable with a finite element coupling as in [8]. Thus, the frequent reservation against the integral approach with reference to the dense matrices is no longer a valid argument [12, 21, 22]. This will be particularly important for $3D$ simulations [21].

6.5. Stabilization and Penalization. The penalty parameter $\varepsilon = h^\alpha$ for $\alpha > 1$ small, such as $\varepsilon = h^{3/2}$ seems to be a good compromise between accuracy (α large) and the condition of the discrete system of equations (α small). In contrast to other situations in convexified problems [1] , a further stabilization appears unnecessary. The adaptive multilevel scheme appears to be capable of an effective numerical simulation.

6.6. Future developments. The a posteriori error estimates in this paper show the reliability-efficiency gap for the error estimators μ (expected to be reliable) and η (expected to be efficient). This dramatic lack of error control requires to be overcome in the future for reliable and accurate numerical simulations.

The effective simulation of large soft magnets is presented in this paper. For other situations the effective regimes are unclear, an effective model equation is unknown. It would be very desirable to simulate those regimes with a macroscopic discretization as well.
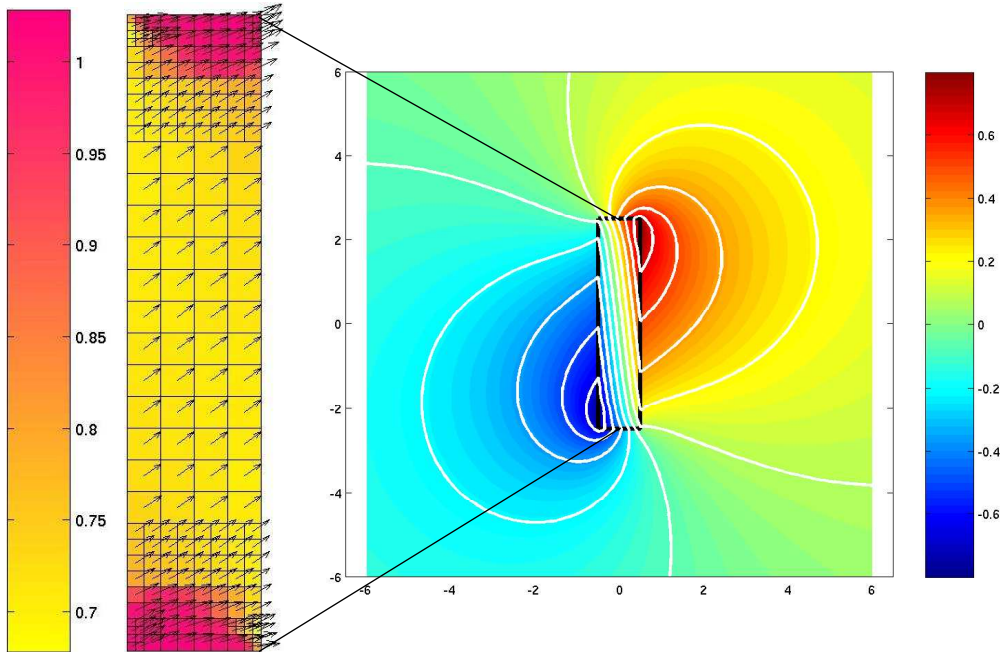
FIGURE 5.11. Discrete Magnetization $\mathbf{m}_h$ (zoom on the left) on the η-adaptively generated mesh $\mathcal{T}_4$ (with $N = 212$) and corresponding potential u_h (right) for constant exterior field $\mathbf{f}^{(2)} = (.5, .5)$ and penalization parameter $\varepsilon = h^{3/2}$. The grey scale in the zoomed magnet displays the length $|\mathbf{m}_h|$ of the discrete magnetization. On the right, the pointwise value of u_h is shown by grey scale and some isolines have been drawn.

Finally, some type of asymptotic expansion of the generic situation for $E_\alpha(\mathbf{m})$ from (1.1) in terms of a very small positive α is very desirable. As the equations change type, continuous trial and test functions of piecewise first-order need to be involved. Higher order discretizations are valuable but rise the difficulty of a conflict with the pointwise side-restriction $|\mathbf{m}| \leq 1$.

REFERENCES

[1] S. BARTELS, C CARSTENSEN, P. PLECHAC, A. PROHL: *Convergence for Stabilisation of Degenerately Convex Minimisation Problems*, preprint 2003.

[2] S. BÖRM, L. GRASEDYCK, W. HACKBUSCH: *Introduction to Hierarchical Matrices with Applications*, Preprint 18/2002, Max-Planck-Institute for Mathematics in the Sciences, Leipzig 2002.

[3] W.F. BROWN: *Micromagnetics*, John Wiley and Sons, New York 1963.

[4] C. CARSTENSEN: *Numerical analysis of microstructure*, Lecture Note 10/2001, Max Planck Institute for Mathematics in the Sciences, Leipzig 2001.

[5] C. CARSTENSEN, K. JOCHIMSEN: *Adaptive finite element error control for non-convex minimization problems: Numerical two-well model example allowing microstructures*, Computing, in press 2003.
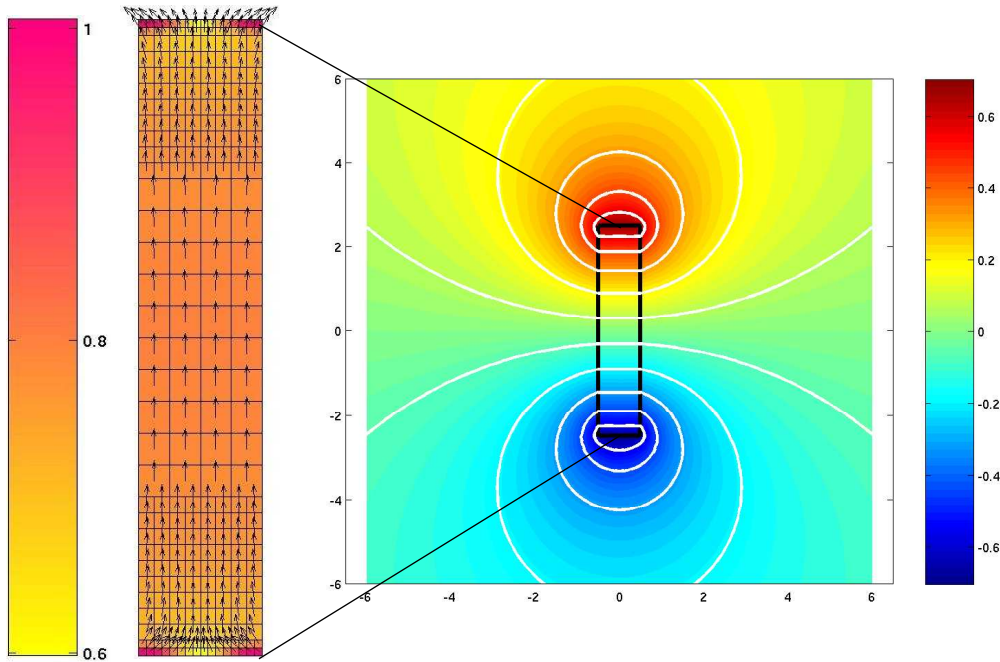
FIGURE 5.12. Discrete Magnetization $\mathbf{m}_h$ (zoom on the left) on the η-adaptively generated mesh $\mathcal{T}_4$ (with $N = 248$) and corresponding potential u_h (right) for constant exterior field $\mathbf{f}^{(3)} = (0, .9)$ and penalization parameter $\varepsilon = h^{3/2}$. The grey scale in the zoomed magnet displays the length $|\mathbf{m}_h|$ of the discrete magnetization. On the right, the pointwise value of u_h is shown by grey scale and some isolines have been drawn.

[6] C. CARSTENSEN, D. PRAETORIUS: *A Posteriori Error Control in Adaptive Qualocation Boundary Element Analysis for a Logarithmic-Kernel Integral Equation of the First Kind*, SIAM J. Sci. Comp., in press 2003.

[7] C. CARSTENSEN, D. PRAETORIUS: *Numerical Analysis for a Macroscopic Model in Micromagnetics*, in preparation 2003.

[8] C. CARSTENSEN, A. PROHL: *Numerical Analysis of Relaxed Micrmagnetics by Penalised Finite Elements*, Numer. Math. 90 (2001), 65-99.

[9] A. DeSIMONE: *Energy Minimizers for Large Ferromagnetic Bodies*, Arch. Rational Mech. Anal. 125 (1993), 99-143.

[10] D. GILBARG, N.S. TRUDINGER: *Elliptic Partial Differential Equations of Second Order*, vol. 224 of *Grundlehren der mathematischen Wissenschaften*, Springer Verlag 1977.

[11] W. HACKBUSCH: *Direct Integration of the Newton Potential Over Cubes Including a Program Description*, Computing 68 (2003), 193-216.

[12] W. HACKBUSCH, J.M. MELENK: $\mathcal{H}$-*Matrix Treatment of the Operator* $\nabla\Delta^{-1}$div, in preparation 2003.

[13] A. HUBERT, R. SCHÄFER: *Magnetic Domains*. Springer-Verlag, Berlin 1998.

[14] R.D. JAMES, D. KINDERLEHRER: *Frustration in Ferromagnetic Materials*, Continuum Mech. Thermondyn. 2 (1990), 215-239.

[15] C.T. KELLEY: *Iterative Methods for Linear and Nonlinear Equations*, Frontiers in Applied Mathematics 16, Philadelphia 1995.

[16] M. LUSKIN, L. MA: *Analysis of the Finite Element Approximation of Microstructure in Micromagnetics*, SIAM J. Numer. Anal. 29 (1992), 320-331.

[17] L. MA: *Analysis and Computation for a Variational Problem in Micromagnetics*, Ph.D. thesis, University of Minnesota 1991.

[18] M. MAISCHAK: *The Analytical Computation of the Galerkin Elements for the Laplace, Lamé and Helmholtz Equation in BEM*, Preprint 1999: *2D BEM*, Preprint 2000: *3D BEM*, Institut für Angewandte Mathematik, Universität Hannover 1999/2000.

[19] J.M. MELENK, S. BÖRM, AND M. LÖHNDORF: *Approximation of Integral Operators by Variable-Order Interpolation*, Preprint 82/2002, Max-Planck-Institute for Mathematics in the Sciences, Leipzig 2002.

[20] P. PEDREGAL: *Parametrized Measures and Variational Principles*, Birkhäuser, Basel 1997.

[21] D. PRAETORIUS: *Analysis, Numerik und Simulation eines relaxierten Modellproblems zum Mikromagnetismus*, Doctorial thesis, Vienna University of Technology 2003.
Submitted thesis available at `http://www.anum.tuwien.ac.at/~dirk/download/dissertation.pdf`

[22] D. PRAETORIUS: *Analysis of the Operator Δ^{-1}div Arising in Magnetic Models*, submitted 2003.
Preprint available at `http://www.anum.tuwien.ac.at/~dirk/download/dpr1x2003.pdf`

[23] D. PRAETORIUS: *Application of $\mathcal{H}$-Matrix Techniques for Micromagnetics*, in preparation 2003.

[24] A. PROHL: *Computational Micromagnetism*, Teubner 2001.

[25] S. SAUTER: *Variable Order Panel Clustering*, Computing 64 (2000), 223-261.

[26] L. TARTAR: *Beyond Young Measures*, Meccanica 30 (1995), 505-526.

E-mail address: `Carsten.Carstensen@tuwien.ac.at`

E-mail address: `Dirk.Praetorius@tuwien.ac.at`

VIENNA UNIVERSITY OF TECHNOLOGY, INSTITUTE FOR APPLIED MATHEMATICS AND NUMERICAL ANALYSIS, WIEDNER HAUPTSTRASSE 8-10, A-1040 VIENNA, AUSTRIA